MODELLING AND CHARACTERIZATION OF A NOVEL GIMBAL TWO-BLADE HELICOPTER ROTOR

Alessandro Croce, Radek Possamai, Alessandro Savorani, Lorenzo Trainelli
Politecnico di Milano, Milano, Italy

Abstract

A novel rotor design specifically conceived for lightweight helicopters is described and analyzed with respect to its kinematic and basic performance characteristics. The design is based on an innovative gimbal mount which allows a quasi-constant-speed transmission from the mast to the hub in a wide variety of relative motions between these two elements. This is motivated by the need of alleviating substantial oscillating rotor loads transmitted to the mast as a result of cyclic flapping. The rotor design is illustrated in detail and the results of several studies are reported, which assess the validity of the proposed design and pave the way to further analysis concerned with the rotor dynamic behaviour.

This paper is dedicated to the memory of dr. Vladimiro Lidak
(1944-2012), Italian helicopter designer and prolific inventor.

1. INTRODUCTION

Lightweight helicopters represent a widespread category of rotorcraft employed in a large variety of roles, ranging from pilot school to sports aviation, aerial work, scouting, and many more. Contrary to larger rotorcraft categories, with their complex design and manufacturing processes, economy considerations and simplicity of operations have led to a markedly lower degree of innovation in this field. As a result, the relatively simple two-blade teetering rotor architecture is still the prevailing design, with its known limitations and drawbacks.

These are especially to be found in the significant 2/rev (two periods per rotor revolution) loads transferred to the mast as a result of rotor cyclic flapping, such as in forward flight or while hovering under gust conditions, which impact considerably on component fatigue life and eventually in maintenance costs. Possible solutions include a radical change in configuration, such as with three-blade fully-articulated designs. However, this is done at the expense of the highly valued characteristics of the two-blade configuration with respect to ease of stowage and transportation, in addition to simplicity and economy.

Among the initiatives towards innovation in light helicopter rotor design, we address the gimballed main rotor head by Dr. Vladimiro Lidak (1944-2012), a missed Italian rotorcraft designer and innovator. Lidak's concept preserves the two-blade configuration, while strongly innovates the rotor head design, introducing an original homokinetic joint below the rotor hub. This joint has been specifically designed to alleviate the 2/rev rotor loads, at a price of a higher mechanical complexity compared to a teetering rotor head. This rotor design was chosen by the K4A S.p.A. Italian company, along with other patented innovative concepts from Dr. Lidak, to be implemented in a novel lightweight two-seat helicopter named KA-2HT which is currently in an advanced development state.

This paper presents a characterization of the kinematics and basic performance characteristics of this novel rotor design based on a high-fidelity modelling of the complete rotor assembly.

2. ROTOR MODEL

2.1. Overview

The main rotor designed for the KA-2HT light helicopter is a two-bladed gimballed, stiff-in-plane rotor. The gimbal joint is the main feature of this design, allowing the hub to rotate freely about the blade teetering and feathering axes. This is obtained through a complex hinge system located within the rotor head. The designer's main goal for this peculiar architecture is the strive for a good approximation of a perfectly homokinetic mast-hub transmission, *i.e.* an ideal linkage providing the equality of the values of the mast and hub angular velocities, irrespective of the latter's tilt with respect to the former.

This characteristic is particularly useful in rotary-wing systems such as helicopters and tilt-rotor aircrafts, because it allows to relief oscillating rotor loads exerted on the rotor shaft. Achieving perfect constant-speed transmission for general (spherical) motions is a complex task and some degree of approximation is usually entrained in rotorcraft gimbal mount designs. Typically, for a given

constant speed of the driving component (mast), one obtains a time-varying, oscillating speed of the driven component (hub) around an average value that is lower than the mast value. Both the difference between the average output and the input speeds and the amplitude of the oscillations are related to the magnitude of the misalignment between the two axes. Of course, the simplest and most approximate gimbal mount is represented by a universal, or Cardan, joint.

In-plane stiffness is the result of the absence of blade lag hinges. The flybar is rigidly connected to the hub central body. It is composed by a transverse bar connected to two short blades, or paddles, provided with typical aerofoil sections, contributing to rotor stability and control through aerodynamic damping. This component is well suited for small helicopters because of its simplicity. Figure 1 provides an overview of this complex rotor head.
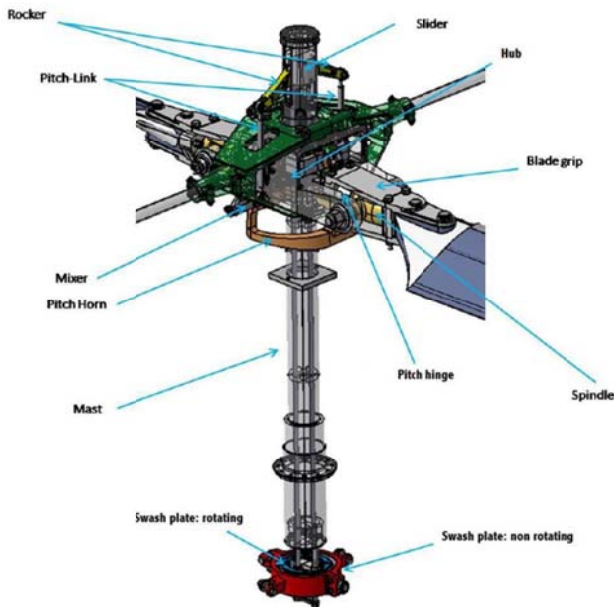
Figure 1. CATIA model of the shaft-rotor head assembly considered in this work (courtesy of K4A S.p.A.).

2.2. Rotor head

The rotor head is the very heart of the design considered in this work. Its gimbal mount consists in a specially devised double Cardan joint with coinciding hinge centres. Double Cardan joints require a centring element able to maintain equal angles between the driven and driving shafts for true constant-speed transmission. This arrangement provides the two gimbal degrees of freedom (teetering and feathering) that allow the hub an arbitrary tilt rotation except for motions around the shaft axis.

A peculiar sequence of mechanical linkages realizes this innovative mount, which aims to approximate a constant-speed joint as much as possible. The first element in this sequence the transmission is the

'carrier' (Figure 2, left). This element is rigidly connected to the mast and is provided with two connections defining a revolute joint that allows the 'internal crosswheel' (Figure 2, centre) to rotate about an axis perpendicular to the mast, corresponding to the feathering degree of freedom. The 'external crosswheel' (Figure 2, right), is joined to the internal one through another revolute joint allowing a relative rotation about an axis perpendicular to the former and the mast, corresponding to the teetering degree of freedom. Therefore, while the internal crosswheel rotates about a single axis, the external crosswheel is subjected to a combination of two relative rotations when referred to the mast.
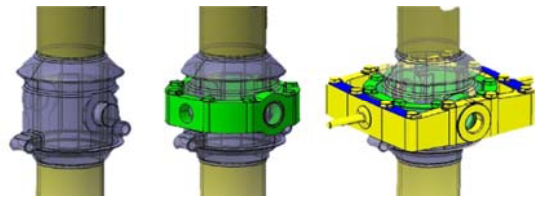
Figure 2. Components of the gimbal mount: carrier (grey), internal crosswheel (green), and external crosswheel (yellow) (courtesy of K4A S.p.A.).

In turn, the external crosswheel is connected to the hub central body by a revolute joint obtained through a pair of holes engaging two pins protruding from the inner part of the hub central body. Furthermore, two additionally pins protrude from the outer part of the external crosswheel. These represent a runner device for two scissor-shaped mechanisms termed the bisectors (Figure 3).
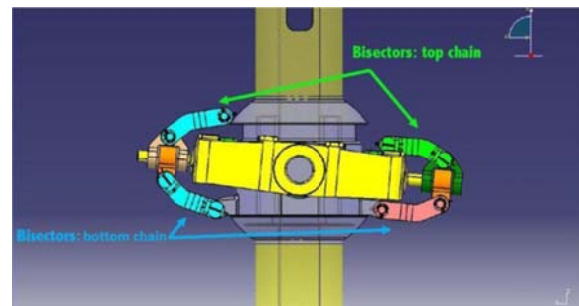
Figure 3. The bisector arrangement (courtesy of K4A S.p.A.).

Each one of these identical devices, symmetrically arranged on the two sides of the external crosswheel, is composed by two subsystems termed the upper and lower chains. The upper bisector chain provides a complex link from the hub central body to the bisector pin through two smaller bodies. The first body can rotate relatively to the hub about an axis perpendicular to the bisector pin and the mast, and relatively to the second about a second axis parallel to the first. Finally, the second body is allowed to freely translate along and rotate about the bisector pin axis, thus realizing a cylindrical joint. The lower bisector chain provides an analogous link, but this time from the carrier to the bisector pin. The two corresponding bodies coupled with the bisector

pin through cylindrical joints are further constrained to translate together.

This complex arrangement, patented by Dr. Lidak [1] is designed to constrain the hub motions in order to obtain the constant-speed transmission. This is achieved by enforcing a nearly constant ratio between relative rotations among some of the system components, thus reducing the number of the effective degrees of freedom from three (those corresponding to the sequenced revolute joints) to two. Indeed, the bisectors basically impose the relative rotations between carrier and external crosswheel and between external crosswheel and hub to assume the same values. In other words, referred to the mast, the relative rotation of the external crosswheel is half that of the hub about the feathering axis. On the other hand, the hub relative rotation about the teetering axis is the same as that of the external crosswheel.

Through the described setup, the bisector pin axis actually bisects the angle formed by the mast and the hub axis normal to the rotor plane, thus approximating a homokinetic transmission.

2.3. Control system

The blade pitch control is achieved by a combination of two independent control actions termed the primary and secondary commands.

The primary command is applied through a standard mechanism in which collective and cyclic pitch control is generated by translation and tilt, respectively, of the non-rotating swashplate. This in turn reflects the pilot cyclic and collective input commands. A pair of control rods, connected to the rotating swashplate, provide the transfer of input motions to the rotor head through a suitable series of linkages ending in two small bodies termed the 'mixers', one for each blade. Figure 4 shows an example of pure primary cyclic command application.
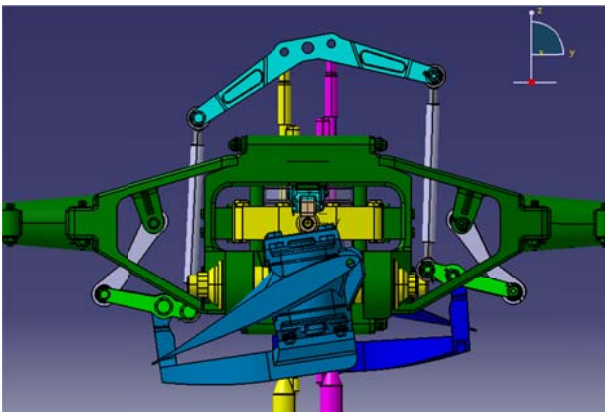
Figure 4. Application of the primary cyclic control with null secondary control (courtesy of K4A S.p.A.).

The secondary command is the result of a mechanical connection between the hub (and

therefore the flybar) and the mixer, reflecting the hub motion about the feathering axis. This additional component of the pitch imposed to the blades involves only cyclic effects. The mixer therefore receives mechanical input from the pitch link, which is the end-effector of the primary command chain, and from the connection to the hub. Figure 5 shows an example of pure secondary command application. The resulting mixer motion is then transferred to the blade by a pitch horn, connected to both mixer and blade through spherical joints.
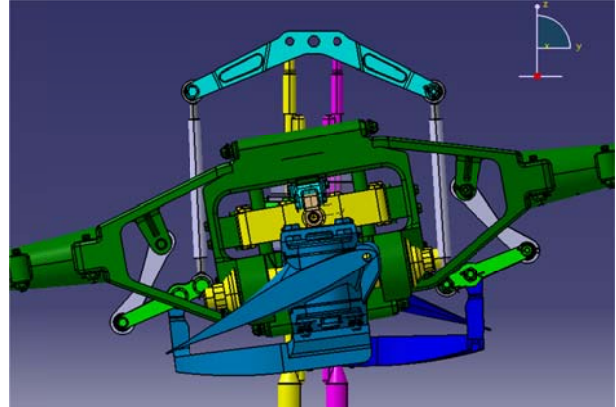
Figure 5. Application of the secondary cyclic control with null primary control (courtesy of K4A S.p.A.).

2.4. Multibody model

In the present work, an effort has been carried out to achieve a high modelling fidelity in order to perform a fully representative, nonlinear kinematic analysis of the hub and blade motions. The rotor system was idealized as a multibody model and implemented in the Cp-Lambda tool [2,3]. The latter is a state-of-the-art finite-element aero-servo-elastic multibody code with a large library of elements including the basic structural elements such as rigid bodies, composite capable beams and shells, and joint models. Joints can be equipped with backlash, free-play and friction models and are modelled through the use of appropriate holonomic or non-holonomic constraints enforced by means of Lagrange multipliers. The code implements special implicit time integration procedures that are non-linearly unconditionally stable [4]. The multibody representation of such a complex system is presented in the following as the assembly of three subsystems comprising numerous rigid bodies and diverse holonomic joints as appropriate.

2.4.1. Rotor head sub-system

The rotor-head subsystem includes several elements that realise the mast-hub transmission. This assembly is symbolically depicted in Figure 6.

As it can be seen, the subsystem model consists of a number of rigid bodies connecting the mast and carrier to the hub by means of two mechanical branches. One goes through a joint to the internal crosswheel, *i.e.* the lower body at point A, the upper

being the external crosswheel. These two bodies rotate relatively to one another about a common hinge centre, as a necessary feature of the present design. The other branch goes through the bisector system. Also this is modelled in a very detailed way, representing all the actual constraints included in its upper and lower chains. Of course, at the modelling level, the redundancy of the bisectors is not needed, since one of them is sufficient to determine the hub motion.
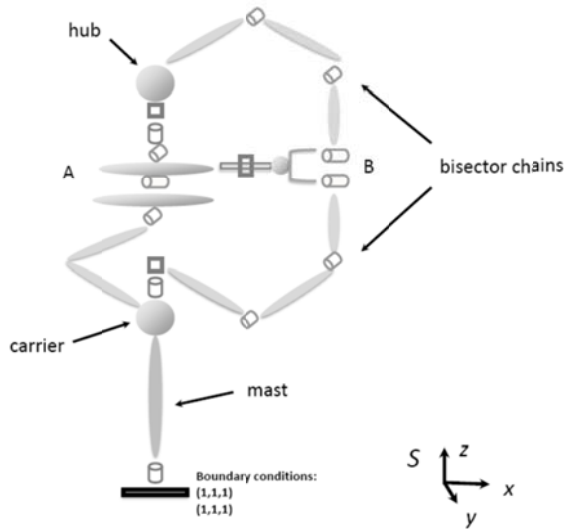
Figure 6. Topological sketch of the rotor-head subsystem.

2.4.2. Control chain sub-system

The control chain subsystem is a complex mechanism providing pitch input to rotor blades. For the sake of clarity, it is presented here separated into two smaller mechanisms: the primary control transfer and pitch application subsystems.
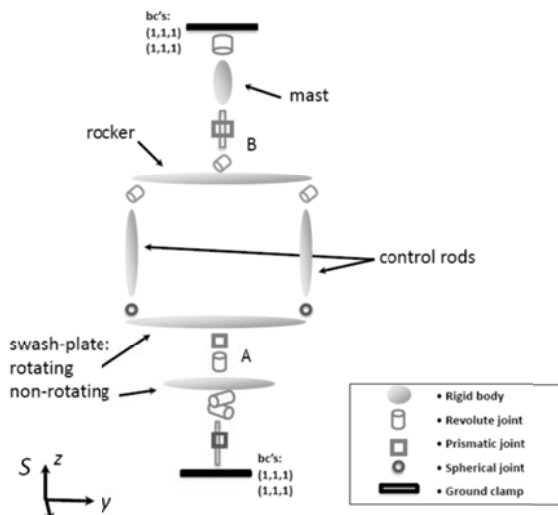
Figure 7. Topological sketch of the primary control transfer subsystem.

The primary control transfer subsystem, depicted in Figure 7, represents the linkage from the non-rotating swashplate to the rotor head, where the body termed 'rocker' is located. This mechanism

includes the non-rotating and rotating swashplates, the control rods, the rocker, the mast and all the necessary joints allowing the transmission of the primary control actions imparted to the non-rotating swashplate up to the rocker. The overall arrangement guarantees a statically determined system with no redundant nor undetermined degrees of freedom. By way of this arrangement, collective pilot inputs are represented by vertical translations of the swashplates through a prismatic joint, and eventually into a translation of the rocker. Cyclic inputs translate into a tilting of the swashplates and correspondingly a tilting of the rocker.

The pitch command application sub-system represents the double mechanism of pitch control application from the rotor head to the blades. This mechanism includes the primary control subchain linking the rocker to the mixer, the secondary control subchain linking the flybar to the mixer, and the final linkage from the mixer to the blade. The latter transfers the mixed pitch command through the pitch horn and the pitch hinge to provide blade feathering around its axis. While the primary pitch control action is transferred to the mixer by way of a rocker motion, the secondary control action derives from flybar tilting, as a result of the hub gimbal motion. The prevailing hub motion component upon blade pitch is that corresponding to the flapping of the flybar, cited above also as hub feathering.
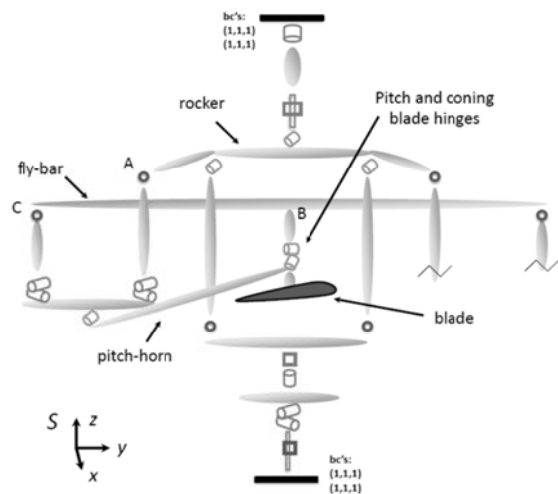
Figure 8. Topological sketch of the complete control chain subsystem.

As seen in Figure 8, the blade motion relative to the hub is not limited to pitching, but includes also coning, through a dedicated hinge. This feature allows the relief of lifting blade loads in operation.

2.4.3. Blades

Eventually, the blades have been modelled as geometrically exact, nonlinear finite element beams capable of accommodating a fully populated stiffness cross-sectional matrix. This allows the static and dynamic analysis of laminated composite

blades with their tailored cross sectional elastic couplings. No modal reduction is performed, and the full finite element equations are used at all times.

In addition, the blades, as well as the flybar paddles, are endowed with aerodynamic properties that allow the calculations of aerodynamic loads. The modelling adopted in the Cp-Lambda code is based on classical two dimensional strip theory using local airfoil characteristics, accounting for the aerodynamic center offset, twist, sweep, and unsteady corrections. The model is completed by a 3-D correction implementing the dynamic inflow model with a variable number of states [2,3].

The subsystems described above are easily linked together in the multibody framework provided by the Cp-Lambda code. In fact, connecting the primary control transfer and pitch command application subsystems via the rocker element, the complete control chain subsystem is obtained, as seen in Figure 8. Finally, this is connected to the rotor-head subsystem via the mast, obtaining the full rotor assembly. The resulting model includes 59 rigid bodies, 21 beam elements, and 44 joints, for a total number of 1756 degrees of freedom.
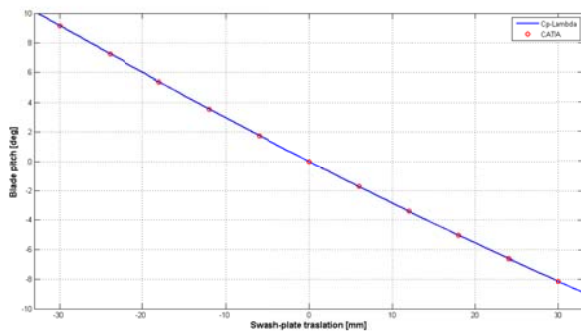
Figure 9. Blade pitch as a function of the swashplate translation (collective command).

3. KINEMATIC STUDIES

The rotor model described above has been verified and analysed by means of a number of kinematic studies. In particular, we considered first the effect of pitch control and flapping actions on the stationary system. Second, we characterised the quality of the constant-speed approximation obtained with the present gimbal mount.

3.1. Control mixing

A preliminary verification of the correctness of the multibody model with respect to geometry and kinematics was performed through a comparison with the CATIA model of the KA-2HT rotor system provided by K4A. Different relative motion inputs were imposed on the rotor system spanning the full range of collective and primary cyclic command, both put into effect by actuating the swashplate. Figures 9 and 10 show the results of the comparison

in terms of the resulting blade pitch.

Analogously, the full span of secondary cyclic command was imposed by flapping the flybar. Figure 11 illustrates the comparison in this case. All instances show an excellent agreement between the two different models, with a maximum mismatch in blade pitch angle barely reaching 1.2%.
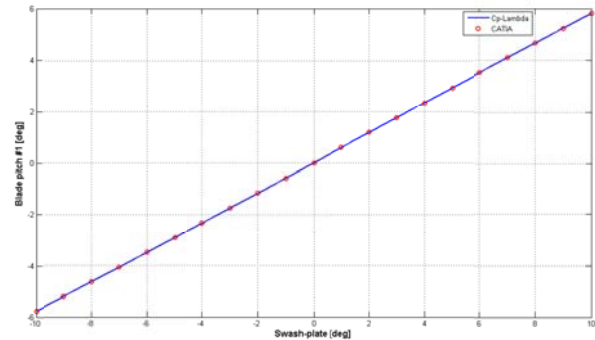
Figure 10. Blade pitch as a function of the swashplate tilt (primary cyclic command).
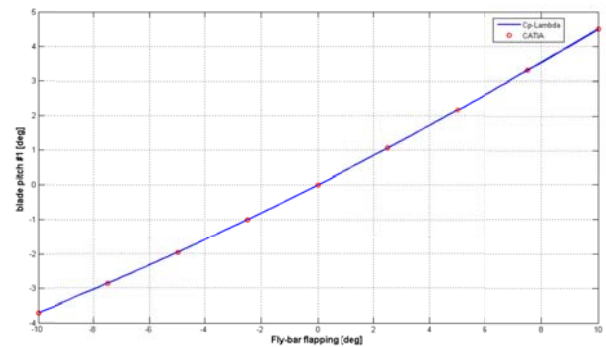
Figure 11. Blade pitch as a function of the flybar tilt (secondary cyclic command).

3.2. Homokinetic behaviour

The constant-speed capability of the gimbal mount considered in this work has been analysed using a similar approach to that presented in [4]. Only the rotor-head subsystem was considered in this case. The numerical experiment was conducted tilting the hub through prescribed rotations, while spinning the mast at constant speed, and measuring the resulting speed component along the hub normal axis. Three different motions were imposed to the hub:

A. banking the hub through a fixed angle referred to rotating mast-fixed axes;

B. oscillating the hub normal in a fixed plane that contains the mast axis;

C. enforcing a conical motion of the hub normal about the mast axis.

In order to perform these tests, some model modifications were required to impose hub motions with respect to a fixed reference frame. Figure 12 shows this modified model where the hub is

connected to the ground by means of two revolute joints whose relative rotations are denoted ϕ_1 and ϕ_2. By imposing suitable prescribed rotations to these joints, the desired planar and conical motions can be enforced.
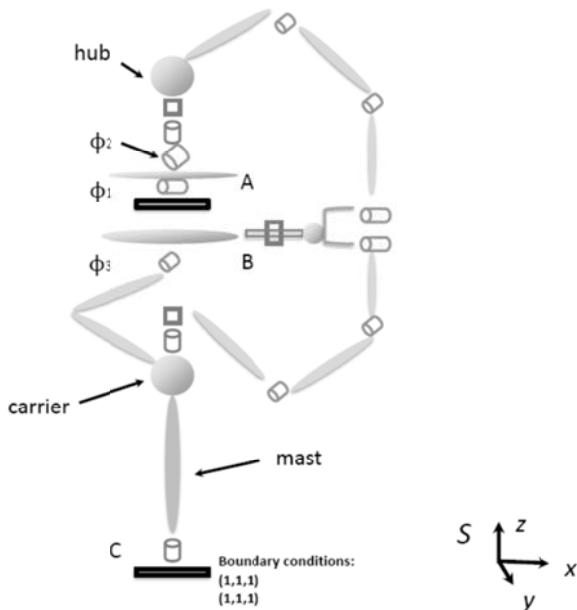
Figure 12. Topological sketch of the rotor-head subsystem modified to perform the constant-speed transmission analysis.

Type A tests were carried out setting a constant relative tilt of 20° between the hub and the mast. This was obtained by enforcing the constant values $\phi_1 = 0°$ and $\phi_2 = 20°$ as seen in Figure 13 (below). In this case, a perfectly homokinetic behaviour was observed, demonstrated in Figure 13 (above), contrary to what would be delivered if using a Cardan joint (Figure 14).
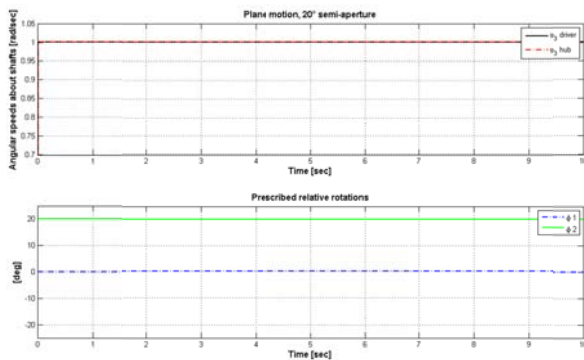
Figure 13. Time histories of the mast and hub rotational speeds (above) and relative rotation (below) for planar oscillating motion.

Type B tests were carried out setting the hub oscillation amplitude to 20°, with null mean value. Oscillations were considered at 2/rev and 4/rev frequency values. This was obtained by enforcing the constant value $\phi_1 = 0°$ and a cosine function for ϕ_2 with amplitude equal to the desired semi-aperture and with the same frequency. An example of the

input functions for the 20°, 4/rev case is given in Figure 15 (below). In this case also, a perfectly homokinetic behaviour was observed, as shown in Figure 15 (above).
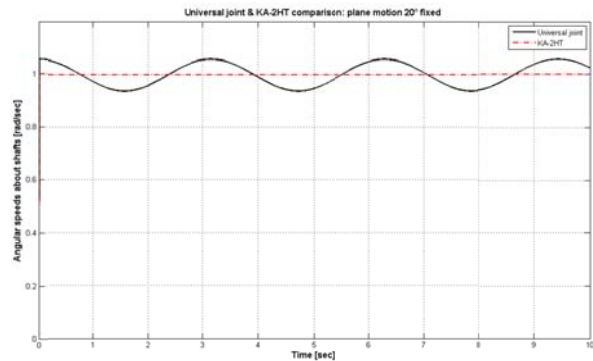
Figure 14. Time histories of the hub rotational speeds for the present design (red dash-dotted line) and the Cardan joint (black line).
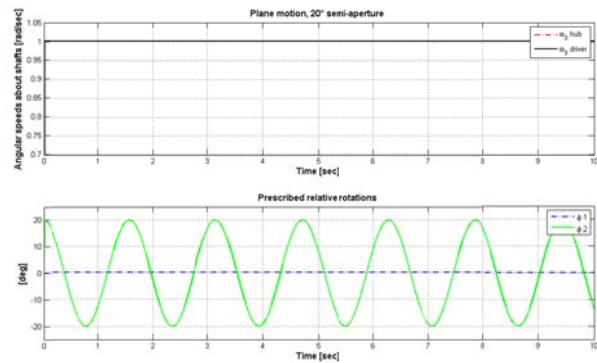
Figure 15. Time histories of the mast and hub rotational speeds (above) and relative rotation (below) for the 20°, 4/rev planar oscillating motion.

Type C tests were carried out enforcing several different motions describing cones of θ = 5°, 10°, 15°, and 20° semi-aperture, at 2/rev and 4/rev precession frequencies. This was obtained by enforcing a cosine function for ϕ_1 with amplitude equal to the desired semi-aperture and with the same frequency, and $\phi_2 = acos(cos(\theta)cos(\phi_1))$. In this case, the homokinetic behaviour is not perfectly achieved. In fact, the hub speed presents an oscillating behaviour and its average value is lower than the mast speed. Increasing the cone semi-aperture and/or the frequency of the precession motion induces a progressive degradation on the constant-speed transmission performance.

This phenomenon is depicted in Figures 16 and 17 in the case of 2ev and 4/rev conical motions with varying semi-aperture values, respectively. In Figure 16, a loss of 3% in average hub speed is observed for the 10° semi-aperture conical motion, growing to 7% for 15° semi-aperture and to 12% for a sizeable 20° semi-aperture. Also, the amplitude of hub speed oscillations are contained below 0.2% at 10° semi-aperture, growing to less than 2% at 20°. It is worth

noting that the foreseen dynamic behaviour of the present rotor when cyclic control is applied involves a 2/rev wobbling response with typical hub tilt amplitude values within 10°. Therefore, the approximation of an ideal constant-speed transmission appears fairly good in the operational range of interest, both in the preservation of the angular speed value and in the ability to restrict periodic variations within a revolution. This favorable behavior is at the root of the positive dynamic characteristics discussed in another study, see [6], where an improvement is observed in oscillating blade load transfer to the airframe compared to other rotor head architectures.
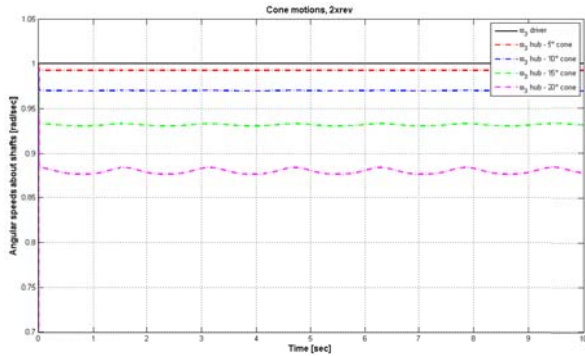
Figure 16. Time histories of the mast and hub rotational speeds for the 5°, 10°, 15° and 20°, 2/rev conical motions.
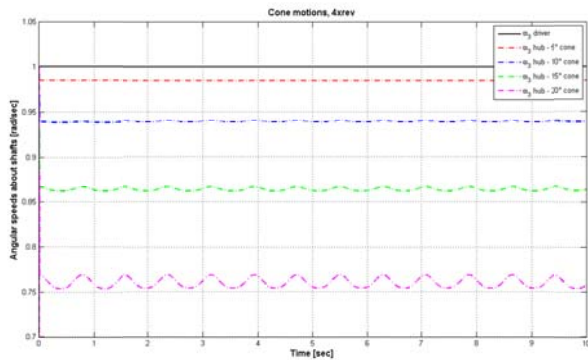
Figure 17. Time histories of the mast and hub rotational speeds for the 5°, 10°, 15° and 20°, 4/rev conical motions.
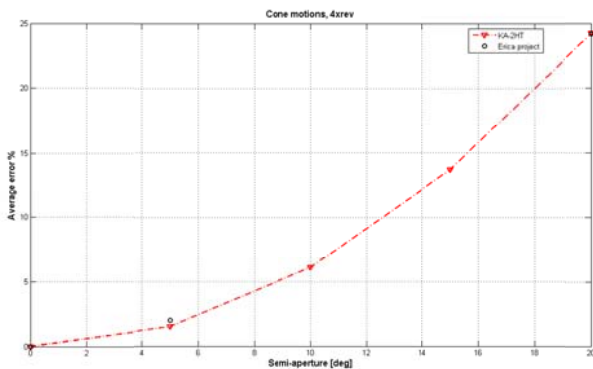
Figure 18. Comparison between the constant-speed transmission performance between the present design and the AgustaWestland 'artichoke' in the case of 20°, 4/rev conical motions.

Furthermore, a comparison with the 'artichoke' gimbal design adopted in the AgustaWestland 'Erica' tilt-rotor project described in [5] was carried out. With respect to 20°, 4/rev cone motions, the two models are very close, with a slight advantage on the side of Lidak's design at lower semi-aperture values, as seen in Figure 18.

4. ROTOR PERFORMANCE

To complete the considered rotor characterisation, a performance analysis was carried out to determine fundamental quantities such as the rotor figure of merit, the power loading, the thrust coefficient and the torque coefficient.

4.1. Figure of merit and power loading

The rotor figure of merit is an important performance index related to the efficiency of the hovering condition. The figure of merit FM is defined as the ratio of the ideal power and the actual power expended to hover at a given weight, where the ideal power is computed by means of the simple momentum theory, while the actual power results from the multibody model in steady-state conditions. We explored the range from 70% of the nominal minimum weight to 170% of the nominal maximum weight values considered for the KA-2HT helicopter.
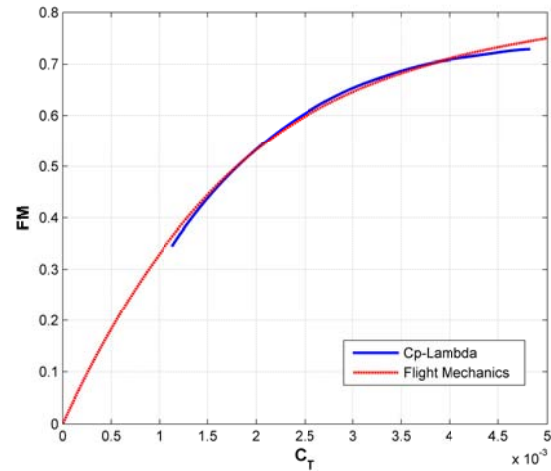
Figure 19. Figure of merit as a function of the thrust coefficient for the Cp-Lambda model (blue), compared to a flight mechanics simulation model (red).

Figure 19 illustrates the rotor figure of merit plotted against the rotor thrust coefficient C_T. The figure shows a second curve representing the behavior predicted using a flight mechanics simulation model for the same rotor based on a formulation following [7]. Although similar, it is possible to appreciate a certain mismatch between the curves as a result of the finely detailed modelling reached within the present multibody framework.

As a further element for performance assessment, we calculated also the power loading PL, defined as

the ratio of thrust to power, and compared its behavior with weight variation to that of the figure of merit FM. This is reported in Figure 20, which shows that, although the figure of merit reaches a maximum at very high weight values, well beyond the operative range, the power loading attains at its peak in vicinity to the higher operative weight values.
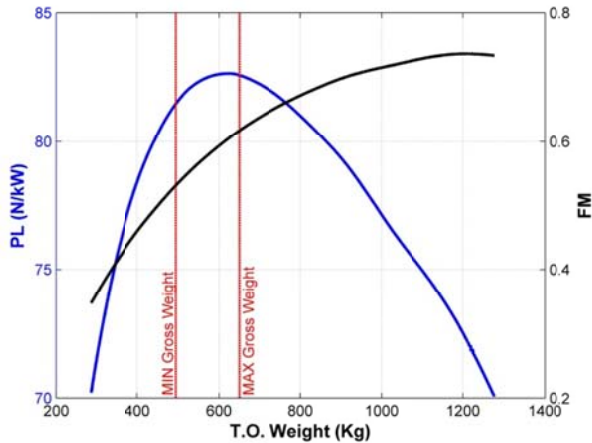
Figure 20. Power loading (blue) and figure of merit (black) as functions of the helicopter weight.

4.2. Thrust/torque curve

Another important performance indicator is the rotor 'polar' curve, *i.e.* the curve that relates the values of the torque coefficient C_Q to those of the thrust coefficient C_T in hover conditions, at different values of the collective pitch. Figure 21 shows the results of the polar curve construction. We considered the comparison between the Cp-Lambda results and those predicted by the flight mechanics simulation model already considered for the figure of merit.
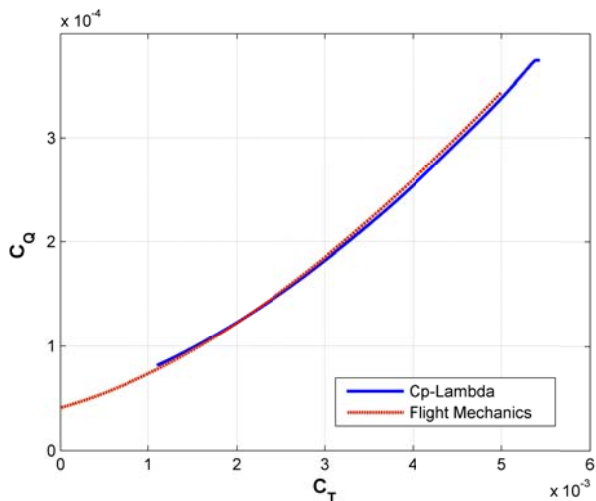
Figure 21. Thrust/torque relationship for the Cp-Lambda model (blue) , compared to a flight mechanics simulation model (red).

Again, a very good agreement is observed, with a slight mismatch that can be justified by the different levels of details in modelling the rotor within the two computational tools.

5. CONCLUDING REMARKS

The present work focused on an innovative rotor design for two-blade lightweight helicopters which is at variance with the well-established pure teetering architecture. The core of the design is represented by Lidak's constant-speed gimbal mount. This complex mechanism, as well as all the other components, has been idealized within the finite element aero-servo-elastic multibody code Cp-Lambda in view of a thorough study of its peculiar dynamic and stability characteristics. The present analysis was limited to geometric and kinematic verification of the model, and to initial performance testing in comparison with other simulation tools, to assess the validity of the modelling hypotheses. Based on these preparatory results, dynamic and stability studies have been carried out, as presented in the companion paper [6]. Furthermore, the present framework allowed the detailed analysis of the constant-speed transmission performance of the gimbal mount. It was verified thus that the design performs very well in several trial nominal motions, including precessional conical motions of the hub with respect to the mast, with very limited time variations between the mast and hub speeds in the operative range of the hub tilting angles. These results confirm Lidak's concept as a promising rotor head arrangement for light rotorcrafts, as an alternative to the traditional teetering mount.

6. REFERENCES

[1] Lidak V., "Constant Velocity Joint for helicopter rotors", patent WO/2010/128378/A2, 2010.

[2] Bauchau O.A., Bottasso C.L., Nikishkov Y.G., "Modeling rotorcraft dynamics with finite element multibody procedures", *Mathematics and Computer Modeling*, **33**, 1113-1137 (2001).

[3] Bottasso C.L., Croce A., Savini B., Sirchi W., Trainelli L., "Aeroelastic Modeling and Control of Wind Turbine Generators Using Finite Element Multibody Procedures", *Multibody System Dynamics*, **16** (3): 291-308 (2006).

[4] O.A. Bauchau, C.L. Bottasso, L. Trainelli. Robust Integration Schemes for Flexible Multibody Systems. *Computer Methods in Applied Mechanics and Engineering*, **192**: 395–420 (2003).

[5] Bottasso, C.L., Trainelli, L., Abdel-Nour, P. e Labò, G., Tilt Rotor Analysis and Design Using Finite-Element Multibody Procedures", 28th European Rotorcraft Forum (ERF 2002), Bristol, UK, September 2002.

[6] Croce A., Possamai R., Trainelli L., "Dynamic Properties of Some Gimbal and Teetering Two-Blade Helicopter Rotor Heads", 40th European

Rotorcraft Forum (ERF 2014), Southampton, UK, September 2014.

[7] Prouty R.W., *Helicopter performance, stability, and control*, PWS engineering, Boston, USA, 1986.

COPYRIGHT STATEMENT